Downloaded from orbit.dtu.dk on: May 04, 2023

DTU Library

# Between ethylene and polyenes--the non-adiabatic dynamics of cis-dienes.

**Kuhlman, Thomas Scheby; Glover, William J; Mori, Toshifumi; Møller, Klaus Braagaard; Martínez, Todd J**

*Published in:*
Faraday Discussions

*Publication date:*
2012

*Document Version*
Publisher's PDF, also known as Version of record

Link back to DTU Orbit

*Citation (APA):*
Kuhlman, T. S., Glover, W. J., Mori, T., Møller, K. B., & Martínez, T. J. (2012). Between ethylene and polyenes--the non-adiabatic dynamics of cis-dienes. *Faraday Discussions*, *157*, 193-212. http://pubs.rsc.org/en/Content/ArticleLanding/2012/FD/c2fd20055d

**General rights**
Copyright and moral rights for the publications made accessible in the public portal are retained by the authors and/or other copyright owners and it is a condition of accessing publications that users recognise and abide by the legal requirements associated with these rights.

- Users may download and print one copy of any publication from the public portal for the purpose of private study or research.
- You may not further distribute the material or use it for any profit-making activity or commercial gain
- You may freely distribute the URL identifying the publication in the public portal

If you believe that this document breaches copyright please contact us providing details, and we will remove access to the work immediately and investigate your claim.

View Article Online / Journal Homepage / Table of Contents for this issue


# Between ethylene and polyenes - the non-adiabatic dynamics of *cis*-dienes†

**Thomas S. Kuhlman,[a] William J. Glover,[bc] Toshifumi Mori,[bc] Klaus B. Møller[a] and Todd J. Martínez*[bc]**

***Received 23rd March 2012, Accepted 30th April 2012***
**DOI: 10.1039/c2fd20055d**

Published on 02 May 2012 on http://pubs.rsc.org | doi:10.1039/C2FD20055D
Downloaded by DTU Library on 07 January 2013

Using Ab Initio Multiple Spawning (AIMS) with a Multi-State Multi-Reference Perturbation theory (MS-MR-CASPT2) treatment of the electronic structure, we have simulated the non-adiabatic excited state dynamics of cyclopentadiene (CPD) and 1,2,3,4-tetramethyl-cyclopentadiene ($Me_4$-CPD) following excitation to $S_1$. It is observed that torsion around the carbon–carbon double bonds is essential in reaching a conical intersection seam connecting $S_1$ and $S_0$. We identify two timescales; the induction time from excitation to the onset of population transfer back to $S_0$ (CPD: ~25 fs, $Me_4$-CPD: ~71 fs) and the half-life of the subsequent population transfer (CPD: ~28 fs, $Me_4$-CPD: ~48 fs). The longer timescales for $Me_4$-CPD are a kinematic consequence of the inertia of the substituents impeding the essential out-of-plane motion that leads to the conical intersection seam. A bifurcation is observed on $S_1$ leading to population transfer being attributable, in a 5 : 2 ratio for CPD and 7 : 2 ratio for $Me_4$-CPD, to two closely related conical intersections. Calculated time-resolved photoelectron spectra are in excellent agreement with experimental spectra validating the simulation results.

## 1 Introduction

Molecules possessing π-electrons play an essential role in organic photochemistry and photophysics.[1] In particular molecules possessing conjugated carbon–carbon double bonds participate in a plethora of reactions induced by light such as photo-isomerisation,[2–11] electrocyclic ring-opening and closing,[12–20] sigmatropic rearrangement[21–23] and cycloaddition.[12,24] Polyenes are prominent examples of such systems *e.g.* retinal, the photoinduced *cis–trans* isomerization of which, initiates the vision process.[25–28] Polyenes also exhibit ultrafast photophysics for example in the light-harvesting and energy-transfer process by carotenoids in the photosynthetic reaction center[29,30] and the non-adiabatic transitions of isolated, longer polyenes such as *all-trans*-2,4,6,8-decatetraene.[31] Thus, fully understanding the intricate nature of the excited state dynamics of polyenes has far reaching implications in photochemistry, photophysics, and photobiology.

[a]*Department of Chemistry, Technical University of Denmark, Kemitorvet 207, DK-2800 Kg, Lyngby, Denmark*
[b]*Department of Chemistry and PULSE Institute, Stanford University, Stanford, California 94305, USA*
[c]*SLAC National Accelerator Laboratory, Menlo Park, California 94309, USA. E-mail: todd.martinez@stanford.edu.*

† Supporting information: Vibrational frequencies of CPD and $Me_4$-CPD and coordinates of optimized geometries for the ground state and MECIs as well as complete ref. 65.

View Article Online

The rich set of photoinduced phenomena exhibited by polyenes is a consequence of the complex nature of the excited states of π-electron systems and conjugated systems in particular. This is evident even in the simplest π-electron system, ethylene, where the lowest $\pi \rightarrow \pi^*$ excited state has zwitterionic character at the Franck–Condon point but diradical character at twisted geometries.[32] For polyenes the picture is even more complicated due to the presence of a low lying (optically dark) electronic state with a large doubly excited character.[33] Due to the dark nature of this doubly excited state it often eludes direct observation, however, it is well established that it plays a significant role in the photochemistry of longer polyenes with more than three conjugated double bonds.[33]

In between the distinct ethylene and the longer polyenes, the role of the doubly excited state in the dienes is more subtle. In the case of *s-trans*-dienes, where the two double bonds are in a *trans*-configuration with respect to the single bond, numerous studies have investigated the state-ordering of the bright $(\pi,\pi^*)$-state and the doubly excited state.[34–40] Both experimental and theoretical studies suggest that the doubly excited state plays a significant role in the initial dynamics following excitation to the bright state giving the *s-trans*-dienes some of the characteristics of the longer polyenes. However, the longer time dynamics resemble that of ethylene.[41–43] In the case of (acyclic) *s-cis*-dienes, fewer studies exist, which is primarily a consequence of the predominance of the *s-trans*-conformation under ambient conditions. For butadiene, for example, the equilibrium concentration at room temperature of the *s-cis*-conformation is only ~3%,[44,45] necessitating very specific experimental conditions for its investigation.[46–48] On the other hand, if the molecule is locked in the *s-cis*-configuration, such as in cyclopentadiene (CPD), experimental investigations are feasible. CPD exhibits intriguing photochemistry such as electrocyclic ring-closure to bicyclo[2.1.0]pent-2-ene and tricyclo[2.1.0.0$^{2,5}$]pentane[49–51] as well as sigmatropic hydrogen shifts.[23] Furthermore, CPD is a prototype molecule for many other five-membered rings containing two double bonds, including heterocycles.

Numerous experimental studies have investigated the low-lying valence states in CPD[52–57] but only few have discussed the spectral position of the doubly excited state.[54,57] Despite the inability to directly locate this dark state in absorption spectroscopy, several time-resolved studies have invoked non-adiabatic transitions involving it to explain the sub 200 fs dynamics observed in ion- and photoelectron signals subsequent to excitation to the bright $(\pi,\pi^*)$-state.[23,58,59] The short timescales involved can also be inferred from the lack of detectable fluorescence of CPD,[60] further hinting at the involvement of a doubly excited state. The timescales of the observed dynamics have furthermore been suggested to be dependent on specific nuclear motion as exemplified in the slow-down of the dynamics from CPD to the substituted 1,2,3,4-tetramethylcyclopentadiene ($Me_4$-CPD).[59]

In this paper, we uncover the specific nuclear dynamics leading to non-adiabatic transitions as well as the connection between static structure and electronic and nuclear dynamics, thereby furthering an understanding of the rules governing excited state dynamics in molecular systems in general. We employ first-principles quantum dynamical methods to investigate the ultrafast excited state dynamics in CPD and $Me_4$-CPD following excitation to the bright $(\pi,\pi^*)$-state. We use the Ab Initio Multiple Spawning (AIMS) method,[61] which can model non-adiabatic effects in a framework that allows simultaneous solution of the electronic structure alongside the nuclear dynamics. We are able to carry out these calculations using an electronic structure method (multi-reference perturbation theory) that can treat both the static and dynamic electron correlation effects that are important in unsaturated and conjugated hydrocarbons.

In the following, we unravel the non-adiabatic nuclear dynamics of CPD and $Me_4$-CPD following excitation to the $(\pi,\pi^*)$-state. The observed dynamics is discussed in light of the dynamics of ethylene and other polyenes, in particular the similar *s-trans*-butadiene. Finally, we relate the results to experimental data from

Published on 02 May 2012 on http://pubs.rsc.org | doi:10.1039/C2FD20055D
Downloaded by DTU Library on 07 January 2013

 This journal is © The Royal Society of Chemistry 2012

time-resolved photoelectron spectroscopy by direct simulation of the experimentally observed signals.

Published on 02 May 2012 on http://pubs.rsc.org | doi:10.1039/C2FD20055D
Downloaded by DTU Library on 07 January 2013

## 2 Theoretical methods

### 2.1 Electronic structure, geometry optimizations and dynamics

Multi-state multi-reference complete active space second-order perturbation theory (MS-MR-CASPT2)[62–64] calculations were performed using the MOLPRO 2006.2 molecular electronic structure package[65] without the use of symmetry, the 6-31G** basis set and a level shift of 0.2 Hartrees. The active space used in all calculations of neutral species consisted of four electrons distributed in four orbitals - the two $\pi$-orbitals and the two lowest lying $\pi^*$-orbitals, with state-averaging over the lowest three singlet states (SA-3-CAS(4,4)). Optimization of stationary points was performed using built-in routines in MOLPRO, whereas optimization of degeneracy points between potential energy surfaces was performed using either the CIOpt code,[66] which uses a penalty function method, or a locally modified version of MOLPRO. Relaxed pathways were calculated using a Nudged Elastic Band (NEB) method.[67,68] The NEB method is conventionally used for finding the minimum energy path between a pair of local minima or stable states, however, here it is used where at least one of the endpoints is not such a configuration. This use of NEB can lead to ambiguity of the path around the endpoint, however, the method is only invoked to demonstrate that barriers present on interpolated paths might not be present if the path is relaxed and as such whether the NEB method converges to the actual minimum energy path is not of importance here.

AIMS calculations were performed using the in-house code combining AIMS dynamics with electronic structure calculations performed in MOLPRO 2006.2[69] at the MS-MR-CASPT2/6-31G** level of theory with state-averaging over three states including analytic MS-MR-CASPT2 non-adiabatic coupling matrix elements.[70,71] The initial positions and momenta of trajectory basis functions (TBFs) were sampled from the 0 K Wigner distribution of the harmonic approximation to the vibrational ground state.[72] The geometry and vibrational frequencies used to obtain the Wigner distribution were calculated at the MP2/6-31G** level of theory in MOLPRO. The initial 40 (24 for $Me_4$-CPD) TBFs were placed on $S_1$ and propagated for 193.5 fs (8000 au) with a time step of 0.39 fs (16 au) using the independent first-generation approximation.[69,73] The final time was chosen long enough to capture the essential dynamics on the excited states.[59] In cases where all population (>99%) had been transferred to the ground state before the final time was reached, the calculation was stopped as our focus here is on the excited state dynamics and timescale of non-adiabatic transfer and not on possible thermal reactions taking place on the vibrationally hot ground electronic state. The dynamics of $Me_4$-CPD was simulated in separate calculations by scaling the mass of $H_{(6)}$–$H_{(9)}$ to match the mass of a methyl group (see Fig. 1). This approximation allows us to

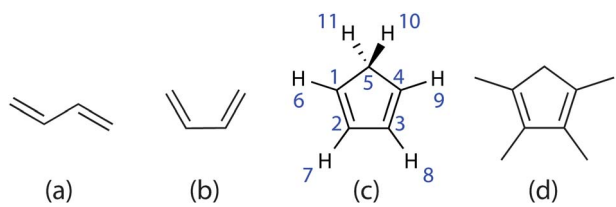


**Fig. 1** Molecular structures of (a) *s-trans*-butadiene, (b) *s-cis*-butadiene, (c) cyclopentadiene (CPD) with numbering, and (d) 1,2,3,4-tetramethylcyclopentadiene ($Me_4$-CPD). Whereas *s-trans*-butadiene belongs to the $C_{2h}$ point group, the three molecules where the double bonds are in an *s-cis*-conformation belong to $C_{2v}$.

View Article Online

separate the effects of changes in mass from changes in the electronic properties upon methylating CPD and is motivated by the experimental observation that the increased density of states due to the methyl groups is not reflected in the dynamics.[59] Nuclear densities were evaluated by Monte Carlo sampling of the pertinent integrals for the desired internal coordinate.[74]

### 2.2 Time-resolved photoelectron spectra

In order to calculate the time-resolved photoelectron spectrum it is necessary to calculate the matrix element connecting the initial $N$-electron neutral state with the final state corresponding to the combination of an $(N-1)$-electron cation state and a continuum electron. In the sudden approximation[75,76] the latter two can be assumed independent, whereby the final state is the product of the cationic and continuum wave functions. In the dipole approximation the matrix element of interest is

$$\left\langle \Psi_I^N(\mathbf{r}_1,\ldots,\mathbf{r}_N)\middle|\hat{\mu}(\mathbf{r}_1,\ldots,\mathbf{r}_N)\middle|\Psi_F^{N-1}(\mathbf{r}_2,\ldots,\mathbf{r}_N)\Psi_{kf}^{el}(\mathbf{r}_1)\right\rangle = \left\langle \phi_{IF}^D(\mathbf{r}_1)\middle|\hat{\mu}(\mathbf{r}_1)\middle|\Psi_{kf}^{el}(\mathbf{r}_1)\right\rangle_{\mathbf{r}_1}, \tag{1}$$

where the equality follows from the strong orthogonality condition between the cation and the ionized electron.[77] $k$ and $f$ label the continuum electron momentum and angular momentum respectively. The Dyson orbital $\phi_{IF}^D$ is given by

$$\left\langle \phi_{IF}^D(\mathbf{r}_1)\right| = \sqrt{N}\left\langle \Psi_I^N(\mathbf{r}_1,\ldots,\mathbf{r}_N)\middle|\Psi_F^{N-1}(\mathbf{r}_2,\ldots,\mathbf{r}_N)\right\rangle_{\mathbf{r}_2,\ldots,\mathbf{r}_N}, \tag{2}$$

where the integration is over all electronic coordinates except for the ones of the ejected photoelectron, $\mathbf{r}_1$. Assuming the electric field of the probe pulse, $\varepsilon_\omega$, to be a $\delta$-function in time and energy (the Bersohn-Zewail model[78]), the time-resolved photoelectron spectrum can be given as a discrete distribution according to

$$\sigma_{\text{stick}}(E_k,\Delta t) \propto \sum_{I,F}\sum_f \left|\left\langle \phi_{IF}^D(\mathbf{r}_1,\Delta t)\middle|\hat{\mu}(\mathbf{r}_1)\middle|\Psi_{kf}^{el}(\mathbf{r}_1)\right\rangle\right|^2 \delta(\hbar\omega - \Delta E(\Delta t) - E_k), \tag{3}$$

where $E_k$ is the kinetic energy of the ejected photoelectron, $\Delta t$ is the time between pump and probe pulses, $\hbar\omega$ is the energy of the probe photon, and $\Delta E$ is the vertical ionization potential from the neutral state $I$ to the cationic state $F$, i.e. the difference in the potential energies $V_I$ and $V_F$ at the center of the neutral state wave packet. The polarization vector of the probe pulse is suppressed in eqn (3) because we compute an isotropic average over all possible relative orientations of the molecule and probe pulse. The above equation is in essence a stick-spectrum. To include the finite extent in time and energy of the probe pulse the stick spectrum is convoluted with a Gaussian $\chi$ in time and energy

$$\sigma(E_k,\Delta t) = \chi(E_{\text{width}},t_{\text{width}}) \otimes \sigma_{\text{stick}}(E_k,\Delta t). \tag{4}$$

The calculations of the photoelectron spectra include the three neutral states employed in the dynamics calculations, as well as two cationic states calculated from MS-MR-CAS(3/4)-PT2 with molecular orbitals taken from the CASSCF solution of the neutral states. The Dyson orbitals were calculated from the neutral and cationic MS-MR-CASPT2 mixing coefficients and CI vectors according to ref. 71, and the transition matrix element was evaluated numerically using the ezDyson code.[79] The latter calculations employed a grid of $192 \times 192 \times 192$ points with a size of $12 \times 12 \times 12$ au$^3$, a maximum angular momentum $f = 7$, analytical isotropic averaging and a Coulomb radial function for the free electron.

Although a high-level, correlated electronic structure method is used in the simulations, inevitably some discrepancy between the energies obtained from calculations and those from experiment is to be expected. Therefore, in order to be able to

Published on 02 May 2012 on http://pubs.rsc.org | doi:10.1039/C2FD20055D
Downloaded by DTU Library on 07 January 2013

 This journal is © The Royal Society of Chemistry 2012

View Article Online

compare the calculated spectra with those from experiment a correction was employed for $\Delta E$ to match to the experimental value of the photoelectron kinetic energy, $E_k$, at the Franck–Condon (FC) point such that $\Delta E \rightarrow \Delta E - \Delta$ with

$$\Delta = [\delta E^{\mathrm{exp.,vert.}}_{S_1 \leftarrow S_0} - \delta E^{\mathrm{CASPT2}}_{S_1 \leftarrow S_0}(\mathbf{Q}_{\mathrm{FC}})] + [\mathrm{IP}^{\mathrm{CASPT2}}_{D_0 \leftarrow S_0}(\mathbf{Q}_{\mathrm{FC}}) - \mathrm{IP}^{\mathrm{exp.,vert.}}_{D_0 \leftarrow S_0}] \quad (5)$$

In eqn (5), $\delta E$ indicates an energy difference between two neutral states, whereas the vertical ionization potential indicated by IP is the energy difference between the neutral ground state and the cationic ground state and $\mathbf{Q}_{FC}$ indicates the FC geometry. This correction ensures that at least the predicted kinetic energy of the photoelectrons ejected from $S_1$ close to time zero matches the experimental value. To determine $\Delta$, the experimental vertical IP of 8.57 eV is used for CPD, and the corresponding value of 7.52 eV for $Me_4$-CPD[80,81] ($\mathrm{IP}^{\mathrm{CASPT2}}_{D_0 \leftarrow S_0} = 8.41$eV). Furthermore, it is assumed that the vertical excitation energy corresponds to the spectral position of the band maximum[59] giving $\delta E^{\mathrm{exp.,vert.}}_{S_1 \leftarrow S_0} = 5.17$ eV for CPD and 4.96 eV for $Me_4$-CPD ($\delta E^{\mathrm{CASPT2}}_{S_1 \leftarrow S_0} = 5.46$eV).

The experimental spectra also exhibit features associated with two-photon ionization, however, the present scheme does not allow for the much more difficult calculation of the two-photon ionization cross-section. As a consequence the probability of two-photon ionization was assumed to be unity for all trajectory basis functions at all times. In other words, we neglect any geometry dependence of the two-photon ionization cross-section and the relative intensity of the one-photon and two-photon ionization spectra are undetermined by our calculations.

Another important factor in simulating the time-resolved photoelectron spectrum is the full-width-at-half-maximum (FWHM) of the experimental cross-correlation (XC) between the pump and probe pulses, which for a one probe and one pump pulse ionization scheme (1 + 1′) was determined to be $\mathrm{FWHM}_{(1+1')} \sim 160$ fs.[59] This value was used for $t_{\mathrm{width}}$ in eqn (4) when calculating the one-photon time-resolved photoelectron spectra. Assuming equal duration of the pump and probe pulse and a Gaussian pulse shape, the FWHM of the XC in a (1 + 2′) ionization scheme is given by $\mathrm{FWHM}_{(1+2')} = \sqrt{\frac{3}{4}} \times \mathrm{FWHM}_{(1+1')} \sim 139$ fs, which was used for $t_{\mathrm{width}}$ when calculating the two-photon spectra. The factor of $\sqrt{\frac{3}{4}}$ results from $\mathrm{XC}_{(1+2')}$ being the outcome of a convolution between a Gaussian and a product of two Gaussians, whereas $\mathrm{XC}_{(1+1')}$ is just the outcome of a convolution between two Gaussians. The spectral bandwidth of the laser pulses was approximately 25 meV and furthermore a detection resolution has to be taken into account.[59] However, due to our limited sampling we used 150 meV for $E_{\mathrm{width}}$ in eqn (4).

## 3 Results and discussion

### 3.1 Electronic structure and potential energy surfaces

In a diene the interaction between the two ethylene units gives rise to two bonding π-orbitals and two anti-bonding π*-orbitals. The ground state configuration, $\pi_1^2\pi_2^2$, is termed $N$, whereas the four possible one-electron promotions give rise to four excited states termed $V_1 - V_4$ by Mulliken (*i.e.* $V_1 - V_4$ are the $(\pi,\pi^*)$-states).[82] For symmetric structures, $V_2$ and $V_3$ will belong to the totally symmetric representation of the pertinent point group, whereas $V_1$ and $V_4$ will belong to $B_u$ and $B_2$ for $C_{2h}$ and $C_{2v}$ respectively (see Fig. 1). Furthermore, a totally symmetric, doubly excited configuration is possible, which will mix with $V_2$, lowering the energy of this state and giving it partial doubly excited character.[54] This doubly excited configuration can be understood as arising from excitation of both of the ethylene units to their lowest triplet states but coupled to an overall singlet.[83] In the following we will use $N$, $V_1$, and $V_2$ as diabatic labels associated with the electronic character of the

Published on 02 May 2012 on http://pubs.rsc.org | doi:10.1039/C2FD20055D
Downloaded by DTU Library on 07 January 2013

View Article Online

state as described here, whereas $S_0$–$S_2$ will be strictly adiabatic labels (*i.e.* denoting only the order of the adiabatic electronic states and not their character).

In the equilibrium ground state geometry of cyclopentadiene (CPD), *i.e.* the Franck–Condon (FC) point, only $H_{(10)}$ and $H_{(11)}$ (see Fig. 1 for numbering) protrude from the plane defined by the five-membered carbon skeleton and the remaining hydrogens, and the molecule possesses an overall $C_{2v}$ symmetry. From the FC geometry, we find the vertical excitation energy to $S_1$ to be 5.46 eV in very good agreement with the best estimate for the vertical transition energy of 5.43 ± 0.05 eV found from a combination of high-level theoretical methods and spectroscopic simulations[84] and in the range 5.19–6.46 eV determined using various high-level electronic structure methods.[85–90] The calculated vertical value is, however, slightly different from the spectral position of the band maximum found from experiment of 5.17–5.33 eV.[52–55,59] At the FC geometry, $S_1$ can be identified as the $V_1$-state characterized by the HOMO → LUMO single $\pi \rightarrow \pi^*$ excitation. Similarly, we find the vertical excitation energy to $S_2$ at this geometry to be 6.51 eV falling in between previous calculated values of 6.31–7.05 eV[85,86,88–90] and slightly above the value of 6.2 eV suggested on the basis of experimental results.[54] The $S_2$ state possesses a large doubly excited character of ~50% primarily due to the HOMO → LUMO double $(\pi)^2 \rightarrow (\pi^*)^2$ excitation and can be identified as the $V_2$-state. The $V_2$-state has not been directly observed in absorption spectroscopy but resonance Raman depolarization ratios suggest that the minimum of this state lies below that of the singly excited $V_1$, and a conical intersection connecting these two states can thus be expected.[57]

Upon excitation from the ground state, the initial nuclear motion will primarily be in the direction of steepest descent along the gradient. In both $S_1$ and $S_2$ the gradient at the FC geometry corresponds closely to movement in the bond alternation coordinate, where the two double bonds contract and the connecting single bond extends (see Fig. 2). If one further examines the gradient for all starting geometries from the initial Wigner sampling an out-of-plane component of the gradient is also observed in some cases, however, the largest component is always in-plane.

Subsequent to the initial nuclear motion along the direction of steepest descent, one could expect motion towards a lower energy configuration on the excited state potential energy surface unless a large momentum leads to motion in a different direction. The minimum energy configurations on the potential energy surface of both excited states located in this work correspond to conical intersections (MECIs) connecting $S_1$ with $S_0$ and $S_2$ with $S_1$ (see Fig. 3 and 4). Two additional MECIs were also located between $S_1$ and $S_0$, which are 39 and 48 meV higher in energy than the minimum energy configuration of $S_1$. Two of the $S_1S_0$-MECIs located in this work, *eth*1-MECI and *eth*2-MECI, result primarily from torsion around a single double bond, wherefore these MECIs are termed ethylene-like, whereas the last, *dis*-MECI, results from a disrotatory mechanism where both double bonds twist to some degree. The double bond torsion might also result in the carbon backbone distortion observed in Fig. 3(a)–(c).

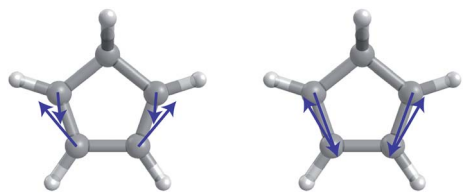


**Fig. 2** Gradient at the FC geometry for $S_1$ (a) and $S_2$ (b). The gradient for both states points in a direction, which leads to a large change of the value of the bond-alternation coordinate defined as $R = R_{12} + R_{34} - R_{23}$ with the numbering given in Fig. 1.

Published on 02 May 2012 on http://pubs.rsc.org | doi:10.1039/C2FD20055D
Downloaded by DTU Library on 07 January 2013

 This journal is © The Royal Society of Chemistry 2012

View Article Online

Published on 02 May 2012 on http://pubs.rsc.org | doi:10.1039/C2FD20055D
Downloaded by DTU Library on 07 January 2013

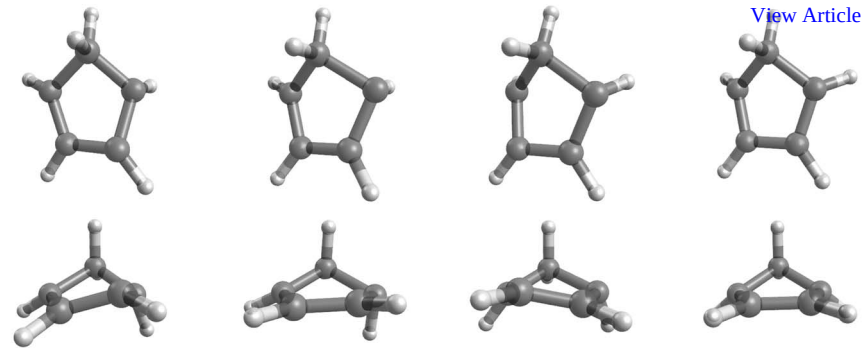

(a) *eth1*-MECI -2.064 eV (b) *eth2*-MECI -2.025 eV (c) *dis*-MECI -2.016 eV (d) $S_2S_1$-MECI -0.636 eV

**Fig. 3** Geometries at the determined minimum energy conical intersections (MECI) viewed from two different angles and relative energies of $S_1$ with respect to the Franck–Condon point. All four MECIs are energetically accessible after photoexcitation to $S_1$.

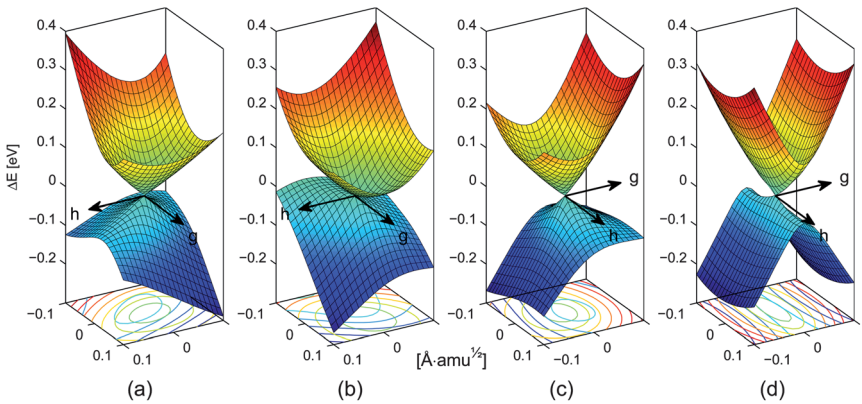


**Fig. 4** Conical intersections in the branching space of the *g*– and the *h*-vector, in mass-weighted displacement, which have been orthogonalized according to the prescription of Yarkony.[92] (a) *eth*1-MECI intersection between $S_1$ and $S_0$, (b) *eth*2-MECI intersection between $S_1$ and $S_0$, (c) *dis*-MECI intersection between $S_1$ and $S_0$, and (d) intersection between $S_2$ and $S_1$.

The potential energy surfaces around the MECIs are illustrated in Fig. 4 along the *g*- and *h*-vectors defining the branching space, where the degeneracy of the two electronic states is lifted to first order. All intersections appear peaked but have different characteristics.[91] Moving away from the degeneracy point of the $S_1S_0$-MECIs, an inspection of the electronic structure shows that the intersections are between a state similar in character to $V_1$ and the ground state $N$, the first being ionic with charge separation between the two carbons of the double bonds (larger charge separation for the most twisted double bond), the second being of a more diradicaloid character. These two states, $V_1$ and $N$, are observed to mix to the largest extent for the *dis*-MECI. The $S_2S_1$-MECI is akin to a crossing of non-interacting diabatic states; one similar to $V_1$ and the other characterized by a large doubly excited character ~60% and thus similar to $V_2$. This latter intersection, which was expected on the basis of experimental findings in ref. 57, leads to $S_1$ possessing the character of $V_2$ in some regions of the potential energy surface.

View Article Online

Downloaded by DTU Library on 07 January 2013
Published on 02 May 2012 on http://pubs.rsc.org | doi:10.1039/C2FD20055D

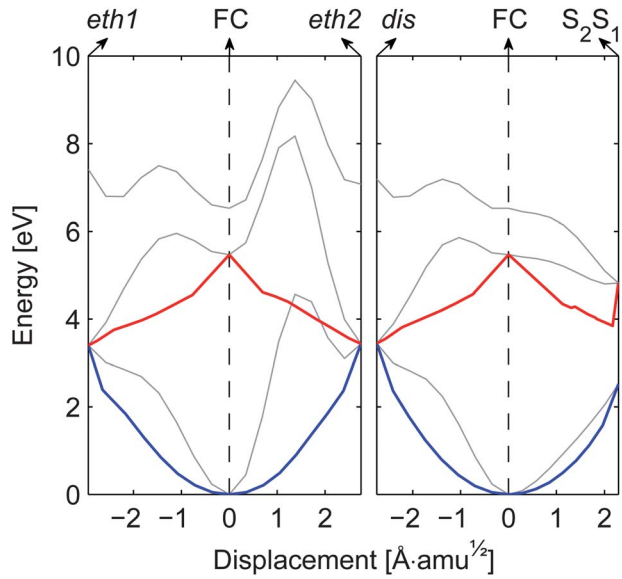


**Fig. 5** Potential energy surfaces connecting the Franck–Condon (FC) geometry with the four minimum energy conical intersections (MECI) as a function of mass-weighted displacement. The thin grey lines represent linearly interpolated surfaces, whereas the thick colored lines represent relaxed paths between the two end points on the given surface from the Nudged Elastic Band algorithm.[67,68] The structures were interpolated from the FC geometry to the MECIs. Consequently, the value on the abscissa is only relevant as a distance to the FC geometry indicated by a dashed vertical line and cannot be used for comparing the distance between two geometries on either side of a vertical line.

To better visualize the connection between the initial FC geometry and the four MECIs, linearly interpolated potential energy surfaces have been calculated for geometries between these points of interest (see Fig. 5). The surfaces can also act as a guide to the intuition on the path followed subsequent to excitation to $S_1$. From the interpolated surfaces it appears there is a barrier on the direct path from the FC geometry to all the $S_1S_0$-MECIs, whereas the path towards the $S_2S_1$-MECI appears to be downhill. If this latter path is followed, the $S_2S_1$-MECI would most likely be passed on the lower half of the cone, see Fig. 4(d), although population transfer to $S_2$ is possible. In this scenario the electronic state character of $S_1$ would thus change from $V_1$ to $V_2$ over the course of the dynamics and population could be transferred back to $S_0$ from this part of the surface at some point along the conical intersection seam. However, if the surfaces are relaxed in directions perpendicular to the direction of the given path the picture changes somewhat (see Fig. 5). On these relaxed paths, shown in bold, the barriers in the direction of the $S_1S_0$-MECIs disappear. Thus, only dynamics calculations can decide whether the part of the $S_1$ potential energy surface of $V_2$-character is visited, and whether the population transfer back to $S_0$ occurs from these $V_2$ regions or if a simpler picture only involving an $S_1$-surface of $V_1$-character is adequate.

## 3.2 Dynamics

**3.2.1 Population transfer - setting the timescales.** From the AIMS calculations it is observed that both CPD and $Me_4$-CPD exhibit ultrafast population decay from the initially excited $S_1$ state back to $S_0$ on a sub 200 fs timescale (see Fig. 6). Very few spawning events from $S_1$ to $S_2$ are observed and the total population transfer to $S_2$ is <0.1%. For both molecules the onset of population decay is, however, preceded by a delay period, the induction time.[93,94] In the case of CPD this period

 This journal is © The Royal Society of Chemistry 2012

View Article Online

Published on 02 May 2012 on http://pubs.rsc.org | doi:10.1039/C2FD20055D
Downloaded by DTU Library on 07 January 2013

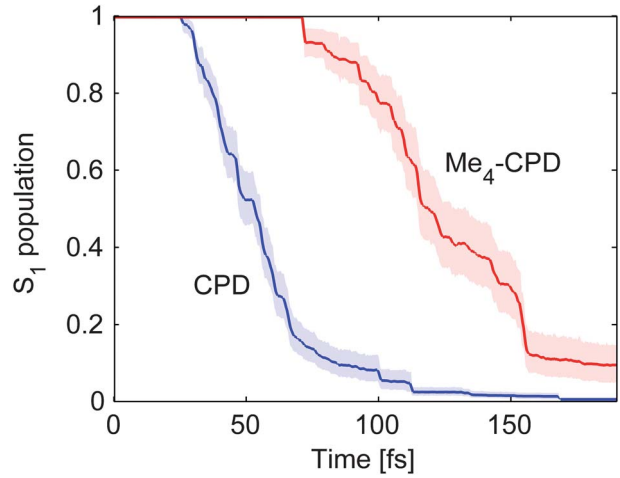


**Fig. 6** Population of the $S_1$ state for CPD (blue) and $Me_4$-CPD (red) with standard deviations from bootstrapping indicated by the shaded regions.

is ~25 fs, while the half-life of the $S_1$ population decay yields a time constant of $\tau_{1/2}$(CPD) ≈ 28 fs. The half-life $\tau_{1/2}$ is defined as the time it takes the S-shaped $S_1$ population curve to reach 0.5 (following the initial induction time).[95] Another option is to fit the population decay to a model such as

$$P(t) = H(t - t_0)\exp(-(t - t_0)/\tau) + H(t_0 - t), \quad (6)$$

where $H$ is the Heaviside step function, $t_0$ is the induction time and $\tau$ is the time-constant of the exponential decay. Due to the non-exponential nature of the population decay, the model in eqn (6) primarily fits the tail of the population falloff. Nonetheless, using such a model gives $\tau$(CPD) ≈ 31 fs and $\tau$(CPD) ≈ 25 fs.

In contrast to CPD, the induction time for $Me_4$-CPD is ~71 fs and $\tau_{1/2}$($Me_4$-CPD) ≈ 48 fs, while the exponential fit yields $t_0$($Me_4$-CPD) ≈ 88 fs and $\tau$($Me_4$-CPD) ≈ 44 fs. The results are thus in line with the experimental observation of a slow down of the non-adiabatic dynamics upon methylation of CPD.[59] The following discussion will explore the background for these observed timescales and their differences.

**3.2.2 In-plane motion.** The initial dynamics following excitation to $S_1$ in both CPD and $Me_4$-CPD is characterized by significant in-plane nuclear motion, as is common in conjugated molecules such as *s-trans*-butadiene,[43] and in line with the observation that the gradient for $S_1$ at the FC geometry corresponds to such motion (see Fig. 2). The promotion of an electron from a bonding π-orbital to an antibonding π*-orbital leads to a weakening of the double bonds, causing an elongation of these in conjunction with a contraction of the $C_{(2)}$–$C_{(3)}$ single bond. This nuclear motion can be quantified by the bond alternation coordinate defined by $R = R_{12} + R_{34} - R_{23}$, the time-dependence of which is given in Fig. 7. A significant in-plane distortion is observed by the rapid increase in this coordinate over the first 15 fs before oscillatory motion around the new equilibrium ensues after ~25 fs. No significant difference is observed between the two molecules as could be expected on the basis of their similar vibrational frequencies for in-plane motion (albeit for the ground state, see Supporting Information†). The mean, about which the coordinate oscillates at later times, of ~1.55 Å for CPD and ~1.54 Å for $Me_4$-CPD is close to the value of 1.54 Å found for the *eth*1-MECI geometry (the coordinate has a value of 1.58 and 1.62 Å for the *eth*2- and *dis*-MECI respectively) and the value of 1.51 Å found for the $S_2S_1$-MECI geometry (see Fig. 3). This indicates that the in-plane

View Article Online

Published on 02 May 2012 on http://pubs.rsc.org | doi:10.1039/C2FD20055D
Downloaded by DTU Library on 07 January 2013

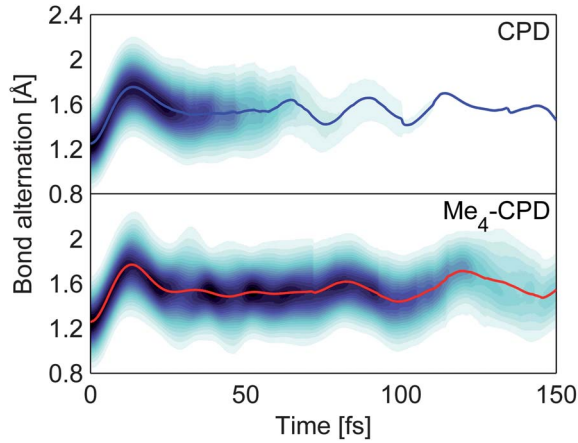


**Fig. 7** Projection of the $S_1$ wavepacket density on the bond alternation coordinate with the expectation value indicated by the colored line for CPD (top, blue) and $Me_4$-CPD (bottom, red). The bond alternation coordinate is defined as $R = R_{12} + R_{34} - R_{23}$ with the numbering given in Fig. 1.

motion towards the intersection with $S_0$ is over within the first ~25 fs and is identical in the two molecules. It is thus evident that the in-plane motion cannot be the source of the different time-scales observed for the population transfer between $S_1$ and $S_0$.

**3.2.3 Out-of-plane motion.** In conjunction with the in-plane nuclear motion, out-of-plane motion is also observed, although this occurs on a longer timescale due to the lower frequency modes involved and since the initial gradient is in the direction of in-plane motion (see Fig. 2). Fig. 8 shows the time-dependence of the backbone torsion given by the absolute value of the dihedral angle $\angle C_{(1)}C_{(2)}C_{(3)}C_{(4)}$. In the case of CPD a steady increase in the expectation value of the backbone torsion is observed over the course of the first ~50 fs before an unstructured behavior takes over. In contrast, it takes ~70 fs before the maximum of the expectation value is reached for the first time in the case of $Me_4$-CPD. Ring deformation through

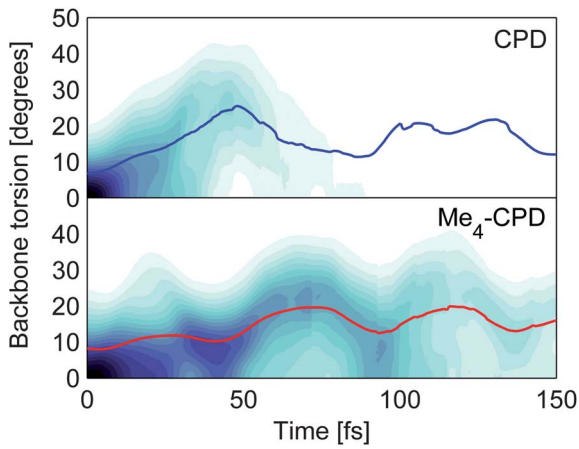


**Fig. 8** Projection of the $S_1$ wavepacket density on the backbone torsion coordinate with the expectation value indicated by the colored line for CPD (top, blue) and $Me_4$-CPD (bottom, red). The backbone torsion is the absolute value of the dihedral angle $\angle C_{(1)}C_{(2)}C_{(3)}C_{(4)}$, with the numbering given in Fig. 1.

 This journal is © The Royal Society of Chemistry 2012

Published on 02 May 2012 on http://pubs.rsc.org | doi:10.1039/C2FD20055D
Downloaded by DTU Library on 07 January 2013

backbone torsion is also observed in the structures of the $S_1S_0$-MECIs in Fig. 3(a)–(c), for which it takes on values of 24.5°, 8.5° and 18.3° for the *eth*1-, *eth*2- and *dis*-MECI respectively. It is thus obvious that ring deformation is essential in reaching the conical intersection seam. The value of the backbone torsion of 24.5° for the *eth*1-MECI is reached within ~50 fs for the expectation value in the case of CPD, whereas it is only reached by a very small part of the population in the case of $Me_4$-CPD. This difference between the two molecules does indicate that the motion in the backbone torsion coordinate is important as a cause of the different time scales for the two molecules, especially in explaining the initial delay period before significant population decay begins. However, from Fig. 8 it is also evident that this cannot be the full story as the expectation value of the backbone torsion drops significantly for CPD after peaking at ~50 fs and the subsequent mean of the coordinate is very similar to that of $Me_4$-CPD and therefore cannot explain the observed slower population decay on a longer time scale.

The geometries of the $S_1S_0$-MECIs are also characterized by a significant torsion in one (or both in the case of the *dis*-MECI) of the double bonds leading to the out-of-plane bend of the $CH_2$-group and a neighboring hydrogen, see Fig. 3. We quantify this torsion as the degree of twist of the most twisted double bond, the time-dependence of which is given in Fig. 9. The value of this coordinate is 50.5°, 58.9°, and 43.4° for the *eth*1-, *eth*2- and *dis*-MECI respectively, whereas it is 31.7° at the $S_2S_1$-MECI. Again we observe a larger degree of out-plane nuclear motion for CPD compared to $Me_4$-CPD on a faster time scale. However, compared to the backbone torsion, it takes >100 fs for the expectation value for $Me_4$-CPD to reach its maximum at ~35°, a value which is obtained after only ~28 fs by CPD. It thus appears that the double bond torsion is essential in reaching the conical intersection seam and combined with distortion of the backbone (which could be a consequence of the double bond torsion) can explain the different time scales observed in the population decay for the two molecules.

From the spawning events we can assign population transfer to one of the $S_1S_0$-MECIs by using the spawning geometries as starting points for optimization of a $S_1S_0$-MECI. This procedure reveals a bifurcation on $S_1$ with 71% and 78% of the population transfer being attributable to the *eth*1-MECI and 27% and 22% to the *eth*2-MECI for CPD and $Me_4$-CPD respectively. For CPD, a very small part of the population, 2%, can be assigned to the *dis*-MECI. This bifurcation is not directly revealed by the overlapping distributions of RMSD between the spawning geometries and the three $S_1S_0$-MECIs (see Fig. 10). The RMSD distributions on the other

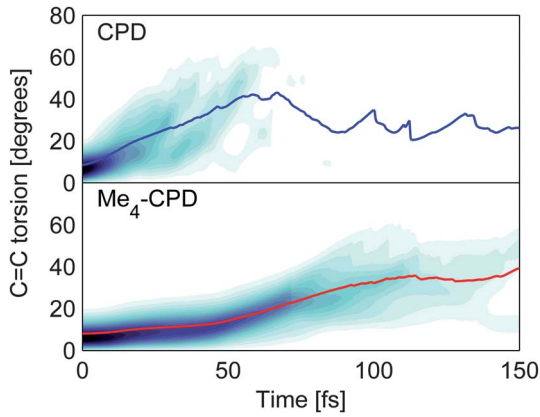


**Fig. 9** Projection of the $S_1$ wavepacket density on the C=C torsion angle (for the most twisted ethylene unit) with the expectation value indicated by the colored line for CPD (top, blue) and $Me_4$-CPD (bottom, red). The torsion is given by $\max[\cos^{-1}((\hat{\mathbf{R}}_{12} \times \hat{\mathbf{R}}_{56})\cdot(\hat{\mathbf{R}}_{12} \times \hat{\mathbf{R}}_{37})),\cos^{-1}((\hat{\mathbf{R}}_{34} \times \hat{\mathbf{R}}_{28})\cdot(\hat{\mathbf{R}}_{34} \times \hat{\mathbf{R}}_{59}))]$, with the numbering given in Fig. 1.

hand do reveal the preference for the ethylene-like MECIs for $Me_4$-CPD, whereas this is not obvious for CPD.

**3.2.4 Electronic character.** Having discussed the nuclear dynamics we turn our attention to the electronic character of the states involved. For the *s-trans*-dienes the two lowest excited states are close in energy at the FC geometry, which for *s-trans*-butadiene has led to the observation of an ultrafast exchange of electronic character between $S_1$ and $S_2$ taking place within the first 5 fs subsequent to excitation to the bright state.[43] This exchange of electronic character is observed by the change in transition dipole moment to $S_0$ such that the initially bright state $S_1$ becomes dark and the initially dark state $S_2$ becomes bright. The change of character is unambiguous for *s-trans*-butadiene. In the case of CPD (and $Me_4$-CPD) the two lowest excited states are separated to a larger extent - at the FC geometry the calculated energy splitting is 1.05 eV, and labels can unambiguously be assigned as the transition dipole moment to $S_1$ is 2.81 D, whereas it is only 0.28 D to $S_2$. Fig. 11 shows the time-development of the ratio of the squared transition dipole moments $\langle|\mu_{01}|^2\rangle/\langle|\mu_{02}|^2\rangle$. For both molecules the ratio starts out >10 (the value is 100 for the FC geometry), however, it drops within the first 10 fs to ~3 and stays at that level. It is thus apparent that there is a mixing of the electronic character, and an unambiguous assignment to bright and dark (or equivalently to $V_1$ and $V_2$) of the two adiabatic states $S_1$ and $S_2$ is not possible at later times.

For *s-trans*-butadiene it is known that charge-transfer states play an essential role in the excited state dynamics.[43] Furthermore, in that molecule charge separation occurs on $S_1$ and is preceded by twisting of a single methylene unit akin to the twist of a single double bond in the cyclopentadienes. In the latter molecules the torsional motion is, however, frustrated due to the ring structure and the twist does not reach the extremum of 90° corresponding to complete out-of-plane twist as is observed in *s-trans*-butadiene. As a consequence a significantly smaller charge separation is observed in the cyclopentadienes.

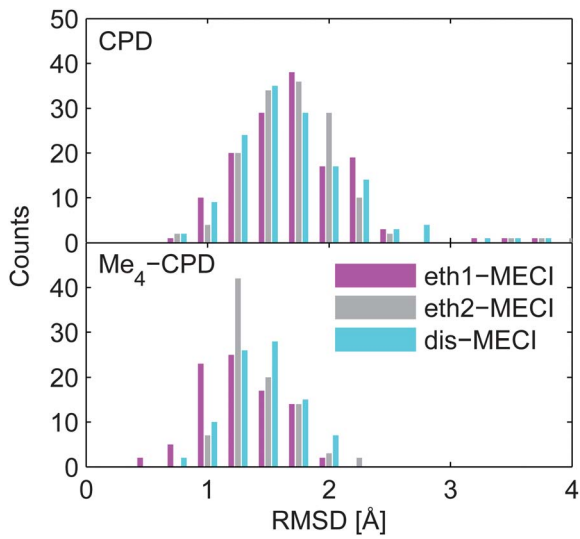


**Fig. 10** Histograms of the RMSD between the spawning geometries and the geometry at the *eth*1-MECI (magenta), the *eth*2-MECI (grey), and the *dis*-MECI (cyan) for CPD (top) and $Me_4$-CPD (bottom).

 This journal is © The Royal Society of Chemistry 2012

Published on 02 May 2012 on http://pubs.rsc.org | doi:10.1039/C2FD20055D
Downloaded by DTU Library on 07 January 2013

View Article Online

Published on 02 May 2012 on http://pubs.rsc.org | doi:10.1039/C2FD20055D
Downloaded by DTU Library on 07 January 2013

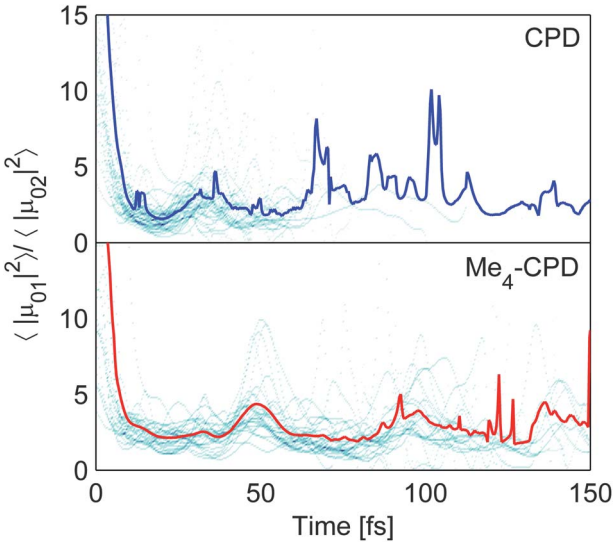


**Fig. 11** Histogram of the ratio of the average of the square of the transition dipole moment between $S_0$ and $S_1$ ($\mu_{01}$) and between $S_0$ and $S_2$ ($\mu_{02}$) with the average value indicated by the colored line for CPD (top,blue) and $Me_4$-CPD (bottom,red). Data is from trajectories on $S_1$ only.

### 3.3 Summary of the excited state reaction mechanism for cyclopentadienes

Having established the nuclear dynamics leading to non-adiabatic transition between $S_1$ and $S_0$ and the electronic character of the states involved, a complete picture of the excited state dynamics emerges and in particular an understanding of the differences between CPD and $Me_4$-CPD and between the cyclopentadienes and *s-trans*-butadiene is established. At the FC geometry, $S_1$ and $S_2$ can clearly be identified as the $V_1$ and $V_2$ states, where the former is primarily a bright, HOMO $\rightarrow$ LUMO singly excited $\pi \rightarrow \pi^*$ state, whereas the latter is a dark state dominated by a large doubly excited character $(\pi)^2 \rightarrow (\pi^*)^2$. Excitation to $S_1$ creates a wavepacket which starts evolving in time. Initial motion primarily along in-plane modes, such as along the bond-alternation coordinate but for CPD also along out-of-plane modes, takes this wavepacket out of the FC region in ~25 fs (see Fig. 12). The motion in the bond-alternation coordinate is typical of conjugated molecules as exemplified by *s-trans*-butadiene.[43] As a consequence of this nuclear motion the wavepacket enters a region of the potential energy surface where the electronic state character mixes significantly and an unambiguous assignment of diabatic labels to the adiabatic states $S_1$ and $S_2$ is no longer possible.

After the initial nuclear motion, additional out-of-plane motion in $Me_4$-CPD occurs from ~25 to ~71 fs after excitation, which is not observed for CPD. This prolonged initial period is a consequence of the slow-down of motion along out-of-plane modes for $Me_4$-CPD compared to CPD due to the inertia of the substituents. This motion in particular involves torsion in the double bonds very similar to that in *s-trans*-butadiene and to the smaller ethylene. Due to the rigid ring structure such motion could have been thought to be absent in the cyclopentadienes but seems to occur nonetheless although slightly suppressed. Although the two ethylene-like $S_1S_0$-MECIs, to which most population transfer can be assigned, primarily result from torsion in only one double bond, the spawning geometries reveal a slight dis-rotatory mechanism, where torsion occurs around both double bonds. The difference in torsion of the two double bonds for most of the spawning geometries falls somewhere in between that for the ethylene-like $S_1S_0$-MECIs and the *dis*-MECI.

View Article Online

Published on 02 May 2012 on http://pubs.rsc.org | doi:10.1039/C2FD20055D
Downloaded by DTU Library on 07 January 2013

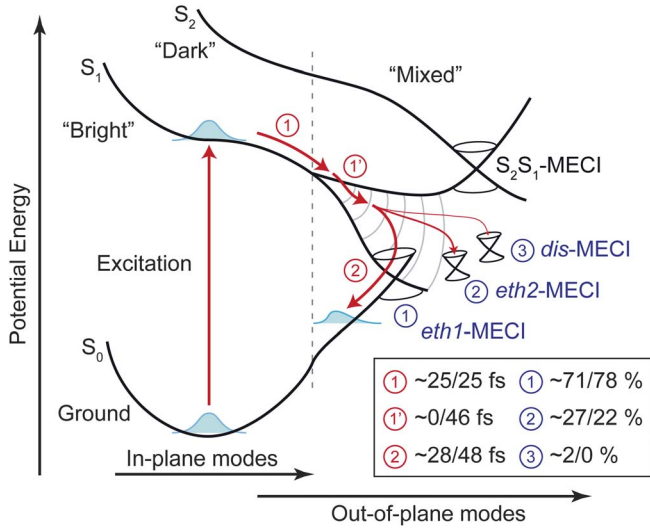


**Fig. 12** Interpretation of the dynamics following excitation to $S_1$ with timescales and branching percentages indicated in the format CPD/$Me_4$-CPD. Initially (1), nuclear motion occurs along in-plane modes such as the bond-alternation coordinate, however, for CPD motion along out-of-plane modes also takes place during this time window. Over the course of the initial nuclear motion the electronic state character mixes making an unambiguous assignment of diabatic labels to $S_1$ and $S_2$ impossible. Following the initial nuclear motion additional out-of-plane motion takes place in $Me_4$-CPD (1′), which is absent in CPD, as a consequence of the slower motion of the former due to the heavy substituents. Finally (2), bifurcation on $S_1$ leads to a non-adiabatic transition primarily assignable to two ethylene-like MECIs.

The out-of-plane motion is thus reminiscent of a reaction path towards a bicyclo [2,1,0]pentene structure and the disrotatory pathway is in accordance with the Woodward–Hoffmann rules.[12] The initial in-plane and out-of-plane motion on $S_1$ *i.e.* the induction time from excitation to the onset of population transfer sets the first timescale of ~25 fs for CPD and ~71 fs for $Me_4$-CPD (see Fig. 12).

After nuclear motion on $S_1$ during the first timescale, the second timescale is set by the non-adiabatic transition back to $S_0$ which takes place with half-lives of $\tau_{1/2}$(CPD) $\approx$ 25 fs and $\tau_{1/2}$($Me_4$-CPD) $\approx$ 48 fs (see Fig. 12). The transition can primarily by assigned to the *eth*1-MECI, which accounts for 71 and 78% of the population transfer for CPD and $Me_4$-CPD respectively, whereas the *eth*2-MECI accounts for 27 and 22% respectively. In the case of CPD, a small population transfer of 2% can be assigned to the *dis*-MECI. An important observation which can be drawn from the determined time-scales is that the slow-down of the non-adiabatic dynamics *i.e.* the longer time-scale of non-adiabatic transition in $Me_4$-CPD compared to CPD is largely accounted for on the basis of the inertia of the substituents and is thus a consequence of a kinematic effect and not due to a difference in the final vibrational density of states (DOS) of $S_0$. From Fermi's Golden rule one would expect a faster transition in the case of $Me_4$-CPD due to a higher DOS, however, recent studies have shown that this can lead to erroneous conclusions regarding the relative rate of transition, and these findings are thus in line with that conclusion.[96] Also, the differences cannot be due to differences in electronic structure, since these are not included in the present simulation.

### 3.4 Femtosecond time-resolved photoelectron spectra

From the nuclear dynamics two time-scales of importance have been identified - one time-scale during which nuclear motion takes place only on the initially excited state with the wavepacket moving away from the FC region, and one time-scale for the

 This journal is © The Royal Society of Chemistry 2012

View Article Online

non-adiabatic transfer back to $S_0$. Using time-resolved photoelectron spectroscopy two time-scales have also been identified experimentally and a comparison between the experiment and the present simulations are found in Table 1. The assignment of the first timescale differs between simulation and experiment and, furthermore, it is observed that the timescales determined from the present simulations are slightly shorter than the ones determined experimentally. The discrepancies in the timescales could be the consequence of approximating the exciting laser pulse by a $\delta$-function in time and energy and the use of the harmonic approximation for constructing the Wigner distribution of the ground state vibrational wave function in the simulations. Both these approximations can lead to an initial wavepacket in the electronic excited state slightly different from the one prepared in the experiments. However, the discrepancies could also partly arise from differences in the method of determining timescales between simulation and experiment. Therefore, to be able to make a direct comparison between theory and experiment and validate the simulations the time-resolved photoelectron spectra are calculated on the basis of the simulated dynamics.

Fig. 13 shows the calculated one-photon spectrum (top), two-photon spectrum (center), and combined spectrum (bottom) of CPD. The combined spectrum has been constructed by assuming the maximum intensity of the one-photon spectrum to be 20 times that of the two-photon spectrum following experimental findings.[59] In accordance with the experimental spectrum,[59] the combined calculated spectrum exhibit a low energy band at $E < 0.5$ eV due to one-photon ionization centered at $t = 0$ and a delayed, broad band due to two-photon ionization (see Fig. 13 (bottom)). Thus, it is evident that the present simulation is able to reproduce the experimental data satisfactorily.

Both bands of the calculated spectrum are observed to originate from ionization out of the same adiabatic state, $S_1$‡. The disappearance of the low-energy, one-photon band is a consequence of a fast increase in ionization potential from $S_1$ to $D_0$, the ground state of the cation, when the wavepacket leaves the FC region and slides down the potential energy surface. It is thus the energetic factor in the last term in eqn (3) that leads to the decay of the low energy band by effectively closing the one-photon probe window. Through two-photon ionization a new probe window is opened further down the potential energy surface resulting in the band centered at a kinetic energy of 1.9 eV. This window stays open longer than the

**Table 1** Comparison between timescales from experimental time-resolved photoelectron spectroscopy[59] and from the present simulations

| | Experimental[a] | | Simulation[b] | |
|---|---|---|---|---|
| Molecule | $\tau$/fs | Interpretation | $\tau$/fs | Interpretation |
| **CPD** | 39 | $S_2 \rightarrow S_1$ transition | 25(31) | Nuclear dynamics on $S_1$ |
| | 51 | $S_1 \rightarrow S_0$ transition | 28(25) | $S_1 \rightarrow S_0$ transition |
| **$Me_4$-CPD** | 68 | $S_2 \rightarrow S_1$ transition | 71(88) | Nuclear dynamics on $S_1$ |
| | 76 | $S_1 \rightarrow S_0$ transition | 48(44) | $S_1 \rightarrow S_0$ transition |

[a] The definition of the $S_1$ and $S_2$ labels in ref. 59 is not identical to the one used throughout this work. [b] The values in parentheses are determined from fitting the $S_1$ population decays using eqn (6).

‡ There is a contribution to the two-photon spectrum <0.75 eV from ionization out of $S_0$ and $S_2$, however, this is hidden below the much stronger one-photon band in the combined spectrum and does not play a significant role when comparing calculation to experiment.

Published on 02 May 2012 on http://pubs.rsc.org | doi:10.1039/C2FD20055D
Downloaded by DTU Library on 07 January 2013

View Article Online

Downloaded by DTU Library on 07 January 2013
Published on 02 May 2012 on http://pubs.rsc.org | doi:10.1039/C2FD20055D

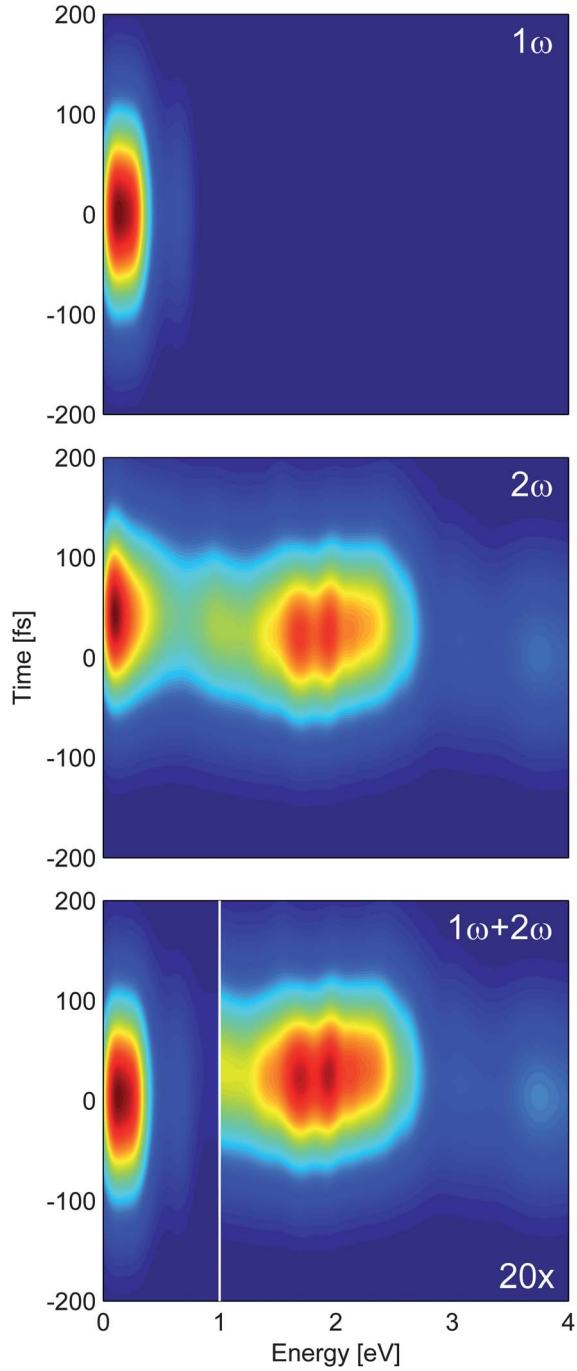


**Fig. 13** Time-resolved photoelectron spectra of CPD. TOP: normalized one-photon spectrum ($1\omega$), center: normalized two-photon spectrum ($2\omega$) and bottom: combined spectrum where the region above 1 eV has been multiplied by a factor of 20 to resemble the presentation of the experimental spectrum in ref. 59. It has furthermore been assumed that the maximum intensity of the one-photon spectrum was 20 times that of the two-photon spectrum in accordance with experimental results.[59]

 This journal is © The Royal Society of Chemistry 2012

View Article Online

Published on 02 May 2012 on http://pubs.rsc.org | doi:10.1039/C2FD20055D
Downloaded by DTU Library on 07 January 2013

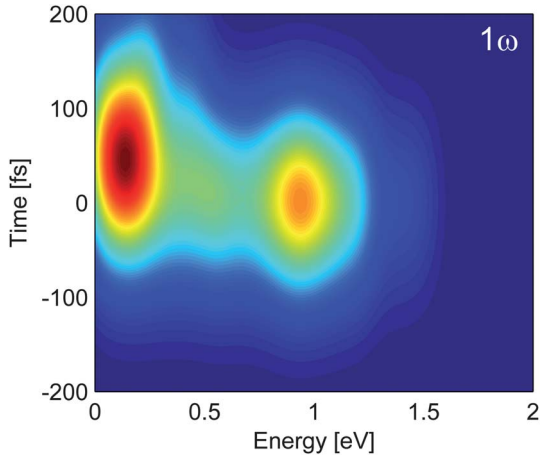


**Fig. 14** One-photon time-resolved photoelectron spectrum of $Me_4$-CPD.

one-photon window until population decay back to the ground state finally leads to the decay of the band.

Fig. 14 shows the calculated one-photon spectrum of $Me_4$-CPD. The spectrum of $Me_4$-CPD was not presented in the experimental work but it was mentioned that the spectrum is similar to that of 5-propyl-cyclopentadiene but red-shifted by 0.1 eV, and this spectrum will therefore be used for comparison. The calculated spectrum in Fig. 14 exhibits two bands, a high energy band centered around 0.95 eV and $t = 0$ and a delayed, lower energy band below 0.3 eV, which is in accordance with what is observed experimentally although the bands are shifted slightly from the experimental values of 1.1 and 0.3 eV§. However, again the present simulation is able to reproduce the experimental data satisfactorily.

Both bands of the calculated spectrum originate from ionization out of the same adiabatic state $S_1$, and one could thus interpret the two bands as a single band moving down in kinetic energy as a function of time as the molecule distorts away from the FC geometry and slides down the potential energy surface. This nuclear motion would lead to an increase in the ionization potential and thus a decrease in kinetic energy of the photoelectrons. By comparing a photoelectron spectrum calculated assuming unit ionization probability with the one in Fig. 14, one can somewhat deduce the cause of the band splitting observed. As the band splitting is apparent in both spectra, the dip separating the band into two is seemingly not due to a change in ionization probability as a consequence of changing electronic character of $S_1$ but most likely a consequence of nuclear dynamics leading to a sudden change in the ionization potential.

## 4 Conclusion

Using Ab Initio Multiple Spawning with electronic structure at the MS-MR-CASPT2 level of theory, we have simulated the excited state dynamics following excitation to $S_1$ in cyclopentadiene (CPD) and 1,2,3,4-tetramethylcyclopentadiene ($Me_4$-CPD). At the Franck–Condon (FC) geometry, $S_1$ is easily identified as resulting from a HOMO $\rightarrow$ LUMO, $\pi \rightarrow \pi^*$ excitation, whereas $S_2$ has a pronounced doubly excited character of $\sim$50%. However, the electronic character mixes significantly as the dynamics unfold on the $S_1$ surface, thus the adiabatic $S_1$ label is not

§ *I.e.* red-shifted by 0.1 eV from the values of 1.2 and 0.4 eV found for 5-propyl-cyclopentadiene.

View Article Online

synonymous with either of the diabatic $V_1$ and $V_2$ labels. Subsequent to excitation, initial motion along the bond-alternation coordinate takes the wavepacket on $S_1$ out of the FC region, whereafter out-of-plane motion ensues due to torsion in the double bonds similar to that of ethylene or *s-trans*-butadiene. The motion is reminiscent of a disrotatory mechanism towards the bicyclo[2,1,0]pentene photoproduct. The induction time from excitation to the onset of significant population transfer back to $S_0$ was determined to be ~25 fs and ~71 fs for CPD and $Me_4$-CPD respectively. The longer timescale for $Me_4$-CPD is due to the inertia of the methyl substituents slowing down the out-of-plane motion essential in reaching the conical intersection seam between $S_1$ and $S_0$ and this slow-down also leads to a longer timescale of non-adiabatic transition. The timescale of non-adiabatic transitions, given by the half-life of the population decay from $S_1$ to $S_0$, were determined to be ~28 fs and ~48 fs for CPD and $Me_4$-CPD respectively.

To make direct connection to experimental observables the time-resolved photoelectron spectra were calculated on the basis of the simulations and were seen to be in correspondence with the experimental spectra. The bands observed in the spectra mainly derive from one- or two-photon ionization out of $S_1$. In the case of CPD the decay of the one-photon band is due to an increasing ionization potential effectively closing the probe window, whereas the two-photon band decays due to population transfer back to $S_0$. As a consequence of the substantially lower ionization potential of $Me_4$-CPD compared to CPD, the one-photon probe window allows for probing of the wavepacket over a longer timescale resulting in the observation of a band shifting down in energy as function of time due to the wavepacket sliding down the $S_1$ potential energy surface. The final decay of the band results from a combination of the probe window closing due to energetic factors as well as population decay back to $S_0$.

Published on 02 May 2012 on http://pubs.rsc.org | doi:10.1039/C2FD20055D
Downloaded by DTU Library on 07 January 2013

## Acknowledgements

This work was supported by the AMOS program within the Chemical Sciences, Geosciences and Biosciences Division of the Office of Basic Energy Sciences, Office of Science, US Department of Energy. T. S. Kuhlman acknowledges financial help from The Danish Ministry of Science, Technology and Innovation through a Elite Research Scholarship during his stay at Stanford University and SLAC National Accelerator Laboratory.

## References

1 N. J. Turro, J. C. Scaiano and V. Ramamurthy, *Modern Molecular Photochemistry of Organic Molecules*, University Science Books, Sausalito, California, 2010.
2 D. H. Waldeck, *Chem. Rev.*, 1991, **91**, 415–436.
3 B. E. Kohler, *Chem. Rev.*, 1993, **93**, 41–54.
4 M. Ben-Nun and T. J. Martinez, *Chem. Phys. Lett.*, 1998, **298**, 57–65.
5 J. Quenneville and T. J. Martinez, *J. Phys. Chem. A*, 2003, **107**, 829–837.
6 T. Schultz, J. Quenneville, B. Levine, A. Toniolo, T. J. Martinez, S. Lochbrunner, M. Schmitt, J. P. Shaffer, M. Z. Zgierski and A. Stolow, *J. Am. Chem. Soc.*, 2003, **125**, 8098–8099.
7 W. Fuß, C. Kosmidis, W. E. Schmid and S. A. Trushin, *Angew. Chem., Int. Ed.*, 2004, **43**, 4178–4182.
8 C. Dugave and L. Demange, *Chem. Rev.*, 2003, **103**, 2475–2532.
9 B. G. Levine and T. J. Martinez, *Annu. Rev. Phys. Chem.*, 2007, **58**, 613–634.
10 L. M. Frutos, T. Andruniow, F. Santoro, N. Ferre and M. Olivucci, *Proc. Natl. Acad. Sci. U. S. A.*, 2007, **104**, 7764–7769.
11 M. Barbatti, M. Ruckenbauer, J. J. Szymczak, A. J. A. Aquino and H. Lischka, *Phys. Chem. Chem. Phys.*, 2008, **10**, 482–494.
12 R. B. Woodward and R. Hoffmann, *The Conservation of Orbital Symmetry*, Verlag Chemie, Weinheim, 1970.
13 W. Fuß, W. E. Schmid and S. A. Trushin, *J. Chem. Phys.*, 2000, **112**, 8347–8362.
14 M. Ben-Nun and T. J. Martinez, *J. Am. Chem. Soc.*, 2000, **122**, 6299–6300.

 This journal is © The Royal Society of Chemistry 2012

View Article Online

15 A. Hofmann and R. de Vivie-Riedle, *J. Chem. Phys.*, 2000, **112**, 5054–5059.
16 M. Garavelli, C. S. Page, P. Celani, M. Olivucci, W. E. Schmid, S. A. Trushin and W. Fuß, *J. Phys. Chem. A*, 2001, **105**, 4458–4469.
17 R. C. Dudek and P. M. Weber, *J. Phys. Chem. A*, 2001, **105**, 4167–4171.
18 F. Rudakov and P. M. Weber, *Chem. Phys. Lett.*, 2009, **470**, 187–190.
19 J. Bao, M. P. Minitti and P. M. Weber, *J. Phys. Chem. A*, 2011, **115**, 1508–1515.
20 S. Deb and P. Weber, *Annu. Rev. Phys. Chem.*, 2011, **62**, 19–39.
21 S. A. Trushin, S. Diemer, W. Fuß, K. L. Kompa and W. E. Schmid, *Phys. Chem. Chem. Phys.*, 1999, **1**, 1431–1440.
22 W. Fuß, W. E. Schmid and S. A. Trushin, *J. Am. Chem. Soc.*, 2001, **123**, 7101–7108.
23 W. Fuß, W. E. Schmid and S. A. Trushin, *Chem. Phys.*, 2005, **316**, 225–234.
24 W. L. Dilling, *Chem. Rev.*, 1969, **69**, 845–877.
25 Q. Wang, R. W. Schoenlein, L. A. Peteanu, R. A. Mathies and C. V. Shank, *Science*, 1994, **266**, 422–424.
26 H. Kandori, Y. Shichida and T. Yoshizawa, *Biochemistry (Moscow)*, 2001, **66**, 1197–1209.
27 D. Polli, P. Altoè, O. Weingart, K. M. Spillane, C. Manzoni, D. Brida, G. Tomasello, G. Orlandi, P. Kukura, R. A. Mathies, M. Garavelli and G. Cerullo, *Nature*, 2010, **467**, 440–U88.
28 T. J. Martinez, *Nature*, 2010, **467**, 412–413.
29 B. P. Krueger, G. D. Scholes, R. Jimenez and G. R. Fleming, *J. Phys. Chem. B*, 1998, **102**, 2284–2292.
30 P. J. Walla, P. A. Linden, C. P. Hsu, G. D. Scholes and G. R. Fleming, *Proc. Natl. Acad. Sci. U.S.A*, 2000, **97**, 10808–10813.
31 V. Blanchet, M. Z. Zgierski, T. Seideman and A. Stolow, *Nature*, 1999, **401**, 52–54.
32 L. Salem, *Science*, 1976, **191**, 822–830.
33 B. S. Hudson, B. E. Kohler and K. Schulten, in *Linear Polyene Electronic Structure and Potential Surfaces*, ed. E. C. Lim, Academic Press, New York, 1982, vol. 6, pp. 1–95.
34 V. Vaida, R. E. Turner, J. L. Casey and S. D. Colson, *Chem. Phys. Lett.*, 1978, **54**, 25–29.
35 L. J. Rothberg, D. P. Gerrity and V. Vaida, *J. Chem. Phys.*, 1980, **73**, 5508–5513.
36 J. P. Doering and R. McDiarmid, *J. Chem. Phys.*, 1980, **73**, 3617–3624.
37 J. P. Doering and R. McDiarmid, *J. Chem. Phys.*, 1981, **75**, 2477–2478.
38 R. McDiarmid and J. P. Doering, *Chem. Phys. Lett.*, 1982, **88**, 602–606.
39 R. R. Chadwick, D. P. Gerrity and B. S. Hudson, *Chem. Phys. Lett.*, 1985, **115**, 24–28.
40 R. R. Chadwick, M. Z. Zgierski and B. S. Hudson, *J. Chem. Phys.*, 1991, **95**, 7204–7211.
41 W. Fuß, W. E. Schmid and S. A. Trushin, *Chem. Phys. Lett.*, 2001, **342**, 91–98.
42 F. Assenmacher, M. Gutmann, G. Hohlneicher, V. Stert and W. Radloff, *Phys. Chem. Chem. Phys.*, 2001, **3**, 2981–2982.
43 B. G. Levine and T. J. Martinez, *J. Phys. Chem. A*, 2009, **113**, 12815–12824.
44 J. G. Aston, G. Szasz, H. W. Woolley and F. G. Brickwedde, *J. Chem. Phys.*, 1946, **14**, 67–79.
45 B. R. Arnold, V. Balaji and J. Michl, *J. Am. Chem. Soc.*, 1990, **112**, 1808–1812.
46 M. E. Squillacote, R. S. Sheridan, O. L. Chapman and F. A. L. Anet, *J. Am. Chem. Soc.*, 1979, **101**, 3657–3659.
47 P. Huber-Wälchli and H. H. Günthard, *Spectrochim. Acta, Part A*, 1981, **37**, 285–304.
48 J. J. Fisher and J. Michl, *J. Am. Chem. Soc.*, 1987, **109**, 1056–1059.
49 J. I. Brauman, L. E. Ellis and E. E. van Tamelen, *J. Am. Chem. Soc.*, 1966, **88**, 846–848.
50 E. E. van Tamelen, J. I. Brauman and L. E. Ellis, *J. Am. Chem. Soc.*, 1971, **93**, 6145–6151.
51 G. D. Andrews and J. E. Baldwin, *J. Am. Chem. Soc.*, 1977, **99**, 4851–4853.
52 L. Pickett, E. Paddock and E. Sackter, *J. Am. Chem. Soc.*, 1941, **63**, 1073–1077.
53 R. P. Frueholz, W. M. Flicker, O. A. Mosher and A. Kuppermann, *J. Chem. Phys.*, 1979, **70**, 2003–2013.
54 R. McDiarmid, A. Sabljic and J. P. Doering, *J. Chem. Phys.*, 1985, **83**, 2147–2152.
55 A. Sabljic and R. McDiarmid, *J. Chem. Phys.*, 1990, **93**, 3850–3855.
56 R. McDiarmid and A. Gedanken, *J. Chem. Phys.*, 1991, **95**, 2220–2221.
57 Q.-Y. Shang and B. S. Hudson, *Chem. Phys. Lett.*, 1991, **183**, 63–68.
58 F. Rudakov and P. M. Weber, *J. Phys. Chem. A*, 2010, **114**, 4501–4506.
59 O. Schalk, A. E. Boguslavskiy and A. Stolow, *J. Phys. Chem. A*, 2010, **114**, 4058–4064.
60 N. Nakashima, S. R. Meech, A. R. Auty, A. C. Jones and D. Phillips, *J. Photochem.*, 1985, **30**, 207–214.
61 M. Ben-Nun and T. J. Martinez, *Adv. Chem. Phys.*, 2002, **121**, 439–512.
62 H.-J. Werner, *Mol. Phys.*, 1996, **89**, 645–661.
63 J. Finley, P. Malmqvist, B. Roos and L. Serrano-Andres, *Chem. Phys. Lett.*, 1998, **288**, 299–306.
64 T. Shiozaki, W. Gyorffy, P. Celani and H.-J. Werner, *J. Chem. Phys.*, 2011, **135**, 081106.

Published on 02 May 2012 on http://pubs.rsc.org | doi:10.1039/C2FD20055D
Downloaded by DTU Library on 07 January 2013

View Article Online

65 H.-J. Werner, P. J. Knowles, R. Lindh, F. R. Manby, M. S., *et al.* MOLPRO, version 2006.1,† a package of ab initio programs, see http://www.molpro.net.
66 B. G. Levine, J. D. Coe and T. J. Martinez, *J. Phys. Chem. B*, 2008, **112**, 405–413.
67 H. Jónsson, G. Mills and K. W. Jacobsen, in *Nudged elastic band method for finding minimum energy paths of transitions*, ed. B. J. Berne, G. Ciccotti and D. F. Coker, World Scientific, 1998, ch. 16, pp. 385–404.
68 D. Sheppard, R. Terrell and G. Henkelman, *J. Chem. Phys.*, 2008, **128**, 134106.
69 B. G. Levine, J. D. Coe, A. M. Virshup and T. J. Martinez, *Chem. Phys.*, 2008, **347**, 3–16.
70 T. Mori and S. Kato, *Chem. Phys. Lett.*, 2009, **476**, 97–100.
71 T. Mori, W. J. Glover, M. Schuurman and T. J. Martinez, *J. Phys. Chem. A*, 2011, **116**, 2808–2818.
72 M. J. Davis and E. J. Heller, *J. Chem. Phys.*, 1984, **80**, 5036–5048.
73 M. D. Hack, A. M. Wensmann, D. G. Truhlar, M. Ben-Nun and T. J. Martinez, *J. Chem. Phys.*, 2001, **115**, 1172–1186.
74 J. D. Coe, B. G. Levine and T. J. Martinez, *J. Phys. Chem. A*, 2007, **111**, 11302–11310.
75 B. T. Pickup and O. Goscinski, *Mol. Phys.*, 1973, **26**, 1013–1035.
76 B. T. Pickup, *Chem. Phys.*, 1977, **19**, 193–208.
77 S. Patchkovskii, Z. Zhao, T. Brabec and D. M. Villeneuve, *Phys. Rev. Lett.*, 2006, **97**, 123003.
78 R. Bersohn and A. H. Zewail, *Ber. Bunsenges. Phys. Chem.*, 1988, **92**, 373–378; J. Petersen, N. E. Henriksen and K. B Møller, *Chem. Phys. Lett.*, 2012, **539-540**, 234–238.
79 L. Tao, C. M. Oana, V. A. Mozhayskiy and A. I. Krylov, *ezDyson*, http://iopenshell.usc.edu/downloads/ezdyson.
80 P. Derrick, L. Asbrink, O. Edqvist, B.-O. Jonsson and E. Lindholm, *Int. J. Mass Spectrom. Ion Phys.*, 1971, **6**, 203–215.
81 V. Kiselev, A. Sakhabutdinov, I. Shakirov, V. Zverev and A. Konovalov, *Zh. Org. Khim.*, 1992, **28**, 2244–2252.
82 R. S. Mulliken, *Rev. Mod. Phys.*, 1942, **14**, 265–274.
83 M. B. Robin, *Higher Excited States of Polyatomic Molecules*, Academic Press, New York, 1975, vol. II.
84 Y. J. Bomble, K. W. Sattelmeyer, J. F. Stanton and J. Gauss, *J. Chem. Phys.*, 2004, **121**, 5236–5240.
85 H. Nakatsuji, O. Kitao and T. Yonezawa, *J. Chem. Phys.*, 1985, **83**, 723–743.
86 L. Serrano-Andrés, M. Merchan, I. Nebot-Gil, B. O. Roos and M. Fülscher, *J. Am. Chem. Soc.*, 1993, **115**, 6184–6197.
87 H. Nakano, T. Tsuneda, T. Hashimoto and K. Hirao, *J. Chem. Phys.*, 1996, **104**, 2312–2320.
88 J. D. Watts, S. R. Gwaltney and R. J. Bartlett, *J. Chem. Phys.*, 1996, **105**, 6979–6988.
89 M. Schreiber, M. R. J. Silva, S. P. A. Sauer and W. Thiel, *J. Chem. Phys.*, 2008, **128**, 134110.
90 J. Shen and S. Li, *J. Chem. Phys.*, 2009, **131**, 174101.
91 D. R. Yarkony, *J. Phys. Chem. A*, 2001, **105**, 6277–6293.
92 D. R. Yarkony, *J. Chem. Phys.*, 2000, **112**, 2111–2120.
93 K. B. Møller and A. H. Zewail, *Chem. Phys. Lett.*, 1998, **295**, 1–10.
94 K. B. Møller, N. E. Henriksen and A. H. Zewail, *J. Chem. Phys.*, 2000, **113**, 10477–10485.
95 K. B. Møller and A. H. Zewail, *Chem. Phys. Lett.*, 2002, **351**, 281–288.
96 T. S. Kuhlman, T. I. Sølling and K. B. Møller, *ChemPhysChem*, 2012, **13**, 820–827.

Published on 02 May 2012 on http://pubs.rsc.org | doi:10.1039/C2FD20055D
Downloaded by DTU Library on 07 January 2013

 This journal is © The Royal Society of Chemistry 2012